Effects of Imperfect Secondary Path Modeling on Adaptive Active Noise Control Systems

Iman Tabatabaei Ardekani, *Student Member, IEEE*, and Waleed H. Abdulla, *Member, IEEE*

***Abstract*—Implementation of adaptive active noise control (ANC) systems requires an estimate model of the secondary path to be uploaded onto digital control hardware. In practice, this model is not necessarily perfect; however, to avoid mathematical difficulties, theoretical analysis of these systems is usually conducted for a perfect secondary path model. This paper conducts a stochastic analysis on performance of Filtered-x LMS (FxLMS)-based ANC systems when the actual secondary path and its model are not identical. This analysis results in a number of mathematical expressions, describing effects of a general secondary path model on stability, steady-state performance and convergence speed of FxLMS-based ANC systems. As a surprising result, it is found that intentional misadjustment of secondary path models can enhance performance of ANC systems in practice. Theoretical results are found to be in a good agreement with the results obtained from numerical analysis. Also, experimental results confirm the validity and accuracy of the theoretical results.**

***Index Terms*—Active noise control (ANS), Filtered-x LMS (FxLMS) algorithm, imperfect secondary path modeling, real time implementation.**

I. Introduction

ACTIVE NOISE CONTROL (ANC) systems are high performance and cost effective alternatives to traditional passive noise control systems [1]. These controllers can be realized using analog or digital electronic technologies; however, realization of adaptive ANC systems is only possible due to digital technology [2]. In order to cope with environmental changes, these systems are implemented using a digital filter updated by an adaptation algorithm. Unfortunately, traditional adaptation algorithms do not show suitable convergence behavior in this application. This is because of the existence of an electro-acoustic channel, called the secondary path, between the ANC controller and the desired silence zone. To compensate for secondary path effects, Filtered-x LMS (FxLMS) algorithm was proposed in the late 1980's [3]–[5]. In this algorithm, the reference signal (acoustic pressure picked up from the ambient) is filtered using an estimate model of the secondary path before being used by the algorithm. Obviously, a major drawback of this algorithm is its need to a secondary path model, which should be obtained using either online or offline secondary path modeling techniques [6]–[8].

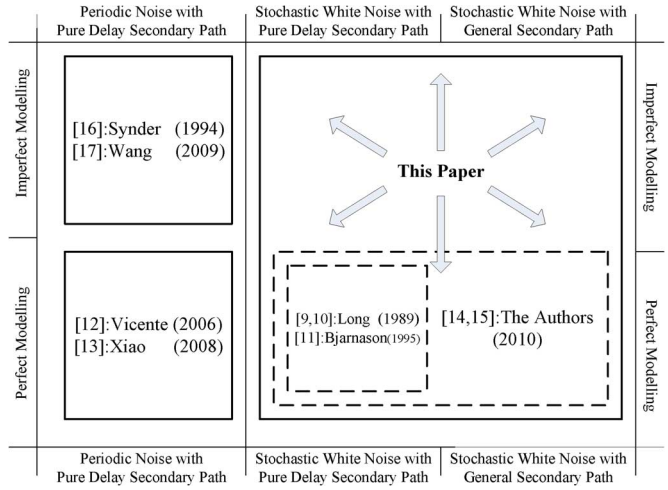

Fig. 1. Existing analyses of FXLMS-based ANC systems performance.

Although performance analysis of FxLMS-based ANC systems have been studied by several researchers [9]–[13], this topic is still an active area of research. Fig. 1 depicts a general view to the research conducted on this subject; also, this figure determines research potentials and open problems. As shown, the authors recently reported two new stochastic analyses on FxLMS-based ANC systems. The first of which focused on the analysis of second-order moments of adaptive variables using Lyapunov stability analysis [14]; and the second of which was based on the analysis of first-order moments of adaptive variables using the root locus method [15]. The common distinction of these two analyses from other existing analyses is that they can apply to any general secondary path. However, similar to other existing studies, both of these studies assumed that the FxLMS algorithm enjoys a perfect secondary path model. As shown in Fig. 1, for simplified cases with pure delay secondary paths and periodic noise, effects of using imperfect secondary path models have been analyzed [16], [17]. However, for a general secondary path and stochastic noise field, these effects have been analyzed only when the secondary path model is assumed to be perfect.

This paper aims to extend the analysis conducted in the authors previous work [14], in order to determine effects of imperfect secondary path models on stability, steady state performance and convergence speed of FxLMS-based ANC systems. As shown in Fig. 1, the distinction of this study from existing studies is that this study assumes a general secondary path and stochastic noise field. The rest of this paper is organized as follows. Section II describes mathematical model of FxLMS-

Manuscript received January 18, 2011; revised April 10, 2011; accepted June 22, 2011. Manuscript received in final form July 04, 2011. Recommended by Associate Editor C. Bohn.

The authors are with the Department of Electrical and Computer Engineering, Faculty of Engineering, The University of Auckland, Auckland 1142, New Zealand.

Color versions of one or more of the figures in this paper are available online at http://ieeexplore.ieee.org.

Digital Object Identifier 10.1109/TCST.2011.2161762

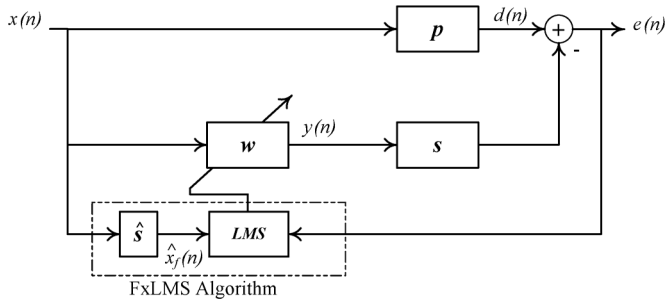

Fig. 2. Block diagram of FxLMS-based active noise control system.

based ANC systems. Section III models dynamics of these systems. Section IV determines effects of imperfect secondary path models on these systems. Section V suggests intentional misadjustment of secondary path models for improving performance of ANC systems. Section VI discusses the validity of theoretical results using numerical analysis. Section VII shows successful application of theoretical results in an experimental ANC setup, implemented using FPGA technology. Section VIII represents concluding remarks.

II. FxLMS-Based ANC Systems

Fig. 2 shows the general block diagram of a single channel FxLMS-based ANC system. In this figure, $x(n)$ is the reference signal, $y(n)$ is the anti-noise signal generated by the ANC controller, $d(n)$ is the acoustic noise in the silence zone, and $e(n)$ is the residual noise in the silence zone. In practice, $x(n)$ is measured using a microphone, called the reference microphone, $y(n)$ is played using a loudspeaker, called the anti-noise source, and $e(n)$ is measured using another microphone, called the error microphone. As shown, $d(n)$ is assumed to be the response of the linear system p to $x(n)$. The ANC controller, which is assumed to be a transversal adaptive filter, is shown by w. The actual secondary path and its model are shown by s and $\hat{s}$, respectively. It is usually assumed that s is a finite-duration impulse response (FIR) system of length Q with an unknown weight vector, represented by

$$\mathbf{s} = [s_0 \quad s_1 \quad \dots \quad s_{Q-1}]^T. \tag{1}$$

This modeling assumption does not cause any constraint to this analysis because actual acoustic signal channels have finite-duration impulse responses. However, even if the actual secondary path has an infinite-duration impulse response (IIR), it can be represented using a FIR system of high order. Similarly, the secondary path model $\hat{s}$ can be described by a FIR system of length $M (M \leq Q)$ with the impulse response represented by weights $\hat{s}_0, \hat{s}_1, \dots, \hat{s}_{M-1}$. This estimate impulse response can be also represented by a $Q \times 1$ weight vector as

$$\hat{\mathbf{s}} = [\hat{s}_0 \quad \hat{s}_1 \quad \dots \quad \hat{s}_{M-1} \quad 0 \quad \dots \quad 0]^T. \tag{2}$$

A. Mathematical Model

According to Fig. 2, for a transversal ANC controller of length L, the residual noise can be expressed as

$$\begin{aligned} e(n) &= d(n) - \sum_{q=0}^{Q} s_q \mathbf{w}^T(n-q)\mathbf{x}(n-q) \\ \mathbf{x}(n) &= [x(n), \dots, x(n-L+1)]^T \\ \mathbf{w}(n) &= [w_0(n), \dots, w_{L-1}(n)]^T \end{aligned} \tag{3}$$

where $\mathbf{x}(n)$ and $\mathbf{w}(n)$ are called the reference and weight vectors, respectively. The residual noise power during the adaptation process, called the mean square error (MSE), is expressed as

$$J(n) = E\left\{e^2(n)\right\}. \tag{4}$$

As shown in [5], the minimal MSE ($J_{\min}$) can be obtained by setting $\mathbf{w}(n)$ to the Wiener–Hopf optimal vector that is

$$\mathbf{w}_o = \mathbf{R}_f^{-1}\mathbf{p}_f \tag{5}$$

where $\mathbf{R}_f = E\{\mathbf{x}_f(n)\mathbf{x}_f^T(n)\}$ and $\mathbf{p}_f = E\{\mathbf{x}_f(n)d(n)\}$. By substituting $\mathbf{w}_o$ into (3) and (4), $J_{\min}$ is obtained as

$$J_{\min} = \sigma_d^2 - \mathbf{p}_f^T\mathbf{R}_f^{-1}\mathbf{p}_f \tag{6}$$

where σ_d^2 denotes the power of $d(n)$. According to (5), $\mathbf{w}_o$ can be computed by using statistical parameters of the noise field; however, these parameters are usually unknown. Avoiding this problem, the FxLMS algorithm which performs a gradient-based adaptation process on $\mathbf{w}(n)$ in such a way that this vector converges to $\mathbf{w}_o$, can be used. This process can be implemented by

$$\mathbf{w}(n+1) = \mathbf{w}(n) + \mu e(n)\mathbf{x}_f(n) \tag{7}$$

where scalar μ is the (adaptation) step-size and vector $\mathbf{x}_f(n)$ is given by

$$\mathbf{x}_f(n) = \sum_{q=0}^{Q-1} s_q \mathbf{x}(n-q). \tag{8}$$

In practice, the weight vector $\mathbf{s}$ is unknown and, therefore, $\mathbf{x}_f(n)$ is estimated by

$$\hat{\mathbf{x}}_f(n) = \sum_{m=0}^{M-1} \hat{s}_m \mathbf{x}(n-m). \tag{9}$$

By replacing $\mathbf{x}_f(n)$ with $\hat{\mathbf{x}}_f(n)$ in (7), the FxLMS algorithm is modified to

$$\mathbf{w}(n+1) = \mathbf{w}(n) + \mu e(n)\hat{\mathbf{x}}_f(n) \tag{10}$$

which can be implemented using the available parameters and the signals collected by the reference and error microphones.

B. Rotated Vectors

Usually, dynamics of FxLMS-based ANC systems are modeled in terms of rotated vectors [18]. These vectors are computed by using the rotation matrix $\mathbf{F}$, obtained from the diagonalization of the auto-correlation matrix $\mathbf{R}$ as

$$\mathbf{R} = E\left\{\mathbf{x}(n)\mathbf{x}^T(n)\right\} = \mathbf{F}\mathbf{\Lambda}\mathbf{F}^T \tag{11}$$

where $\mathbf{F}$ is the eigenvectors matrix, satisfying the equality of $\mathbf{F}^T\mathbf{F} = \mathbf{I}_L$, and diagonal matrix $\mathbf{\Lambda}$ contains the eigenvalues of $\mathbf{R}$. For a broad-band white signal of power σ_x^2, it can be shown that

$$\mathbf{\Lambda} = \sigma_x^2\mathbf{I_L}. \tag{12}$$

Now, the rotated reference vector is defined as

$$\mathbf{z}(n) \triangleq \mathbf{F}^T\mathbf{x}(n). \tag{13}$$

This vector can be also represented in form of

$$\mathbf{z}(n) = [z_0(n) \quad z_1(n) \quad \dots \quad z_{L-1}(n)] \tag{14}$$

$$z_l(n) = \mathbf{F}_l^T\mathbf{x}(n), \quad l = 0, 1, \dots, L-1 \tag{15}$$

where $\mathbf{F}_l^T$ denotes the lth column of $\mathbf{F}$. Similarly, the rotated weight misalignment vector is defined as

$$\mathbf{c}(n) \triangleq \mathbf{F}^T\left[\mathbf{w}(n) - \mathbf{w}_o\right]. \tag{16}$$

This vector can be also represented in form of

$$\mathbf{c}(n) = [c_0(n) \quad c_1(n) \quad \dots \quad c_{L-1}(n)]^T. \tag{17}$$

Equations (3), (9), and (10) can be re-expressed in terms of rotated vectors as

$$e(n) = e_o(n) - \sum_{q=0}^{Q} s_q\mathbf{c}^T(n)\mathbf{z}(n-q) \tag{18}$$

$$\mathbf{c}(n+1) = \mathbf{c}(n) + \mu\hat{\mathbf{z}}_f(n)e(n) \tag{19}$$

$$\hat{\mathbf{z}}_f(n) = \sum_{m=0}^{Q-1} \hat{s}_m\mathbf{z}(n-m) \tag{20}$$

where $e_o(n)$ is the optimal residual noise, obtained by setting $\mathbf{w} = \mathbf{w_o}$ in (3).

C. Independence Assumptions

The independence assumptions, proposed by Gardener [19], are usually used in the stochastic analysis of the FxLMS algorithm, such as those reported in [9]–[11] and [15]. The first independence assumption states that pair $\{\mathbf{x}(n), d(n)\}$ is a zero mean independent identically distributed (iid) sequence; therefore

$$E\left\{\mathbf{x}(n-p)\mathbf{x}^T(n-q)\right\} = \mathbf{R}\delta_{p,q} \tag{21}$$

where $\delta_{m,p}$ is Kronecker delta function. Combining this assumption and (12), (13) results in

$$E\left\{\mathbf{z}(n-m)\mathbf{z}^T(n-p)\right\} = \sigma_x^2\delta_{m,p}\mathbf{I}_L. \tag{22}$$

The second assumptions states that $e_o(n)$ is independent of the noise process [19]. Consequently, $e_o(n)$ is independent of the rotated reference vector $\mathbf{z}$. Finally, the third independence assumption states that for small adaptation step-sizes, adaptive weights are statistically independent of noise samples [5]. Accordingly, rotated misalignment weights and elements of the rotated reference vector are statistically independent.

III. Modeling Convergence Behavior of FxLMS-Based ANC Systems

In [14], it is shown that by substituting (18) into (4) and using the independence assumptions, the MSE function can be expressed as

$$J(n) = J_{\min} + J_{ex}(n) \tag{23}$$

where $J_{\min} = E\{e_o^2(n)\}$ and $J_{ex}(n)$, called the excess-MSE function, is given by

$$J_{ex}(n) = \sigma_x^2\sum_{q=0}^{Q-1} s_q^2E\left\{\mathbf{c}^T(n-q)\mathbf{c}(n-q)\right\}. \tag{24}$$

The time difference of $J_{ex}(n)$ is defined as

$$\triangle J_{ex}(n) \triangleq J_{ex}(n+1) - J_{ex}(n). \tag{25}$$

By combining (19), (24), and (25), $\triangle J_{ex}(n)$ can be obtained as

$$\triangle J_{ex}(n) = \hat{A}(n) + \hat{B}(n) \tag{26}$$

where scalar functions $\hat{A}(n)$ and $\hat{B}(n)$ are given by

$$\hat{A}(n) = \mu^2\sigma_x^2\sum_{q=0}^{Q-1} s_q^2E\left\{e^2(n-q)\hat{\mathbf{z}}_f^T(n-q)\hat{\mathbf{z}}_f(n-q)\right\}$$

$$\hat{B}(n) = 2\mu\sigma_x^2\sum_{q=0}^{Q-1} s_q^2E\left\{\mathbf{c}^T(n-q)\hat{\mathbf{z}}_f(n-q)e(n-q)\right\}.$$

Appendix A shows that $\hat{A}(n)$ can be simplified to

$$\hat{A}(n) = \mu^2\sigma_x^4\|\hat{\mathbf{s}}\|^2L\left(\|\mathbf{s}\|^2J_{\min} + \mathcal{J}(n)\right) \tag{27}$$

where $\mathcal{J}(n)$ is defined as

$$\mathcal{J}(n) \triangleq \sum_{q=0}^{Q-1} s_q^2J_{ex}(n-q). \tag{28}$$

Appendix B shows that $\hat{B}(n)$ can be simplified to

$$\hat{B}(n) = -2\mu\sigma_x^2\frac{\mathbf{s}^T\hat{\mathbf{s}}}{\|\mathbf{s}\|^2}\left(1 - \mu\sigma_x^2\mathbf{s}^T\mathbf{\Psi}_Q\hat{\mathbf{s}}\right)\mathcal{J}(n) \tag{29}$$

where constant matrix $\mathbf{\Psi}_Q$ is defined as

$$\mathbf{\Psi}_Q = \mathrm{diag}(0, 1, \dots, Q-1). \tag{30}$$

Now, substituting (27) and (29) into (26) results in

$$\triangle J_{ex}(n) = \mu\sigma_x^2\|\hat{\mathbf{s}}\|^2\left\{\alpha J_{\min} - \hat{\beta}\mathcal{J}(n)\right\} \tag{31}$$

where coefficients α and $\hat{\beta}$ are given by

$$\alpha = \mu L \sigma_x^2 \|\mathbf{s}\|^2 \tag{32}$$

and

$$\hat{\beta} = 2\frac{\mathbf{s}^T\hat{\mathbf{s}}}{\|\mathbf{s}\|^2\|\hat{\mathbf{s}}\|^2} - \mu\sigma_x^2(L + 2\hat{\Delta}_{eq}). \tag{33}$$

$\hat{\Delta}_{eq}$ is the secondary path equivalent delay, defined as

$$\hat{\Delta}_{eq} = \frac{\mathbf{s}^T\hat{\mathbf{s}}}{\|\mathbf{s}\|^2\|\hat{\mathbf{s}}\|^2}(\mathbf{s}^T\mathbf{\Psi}_Q\hat{\mathbf{s}}). \tag{34}$$

In [14] and [15], the authors defined the concept of secondary path equivalent delay (Δ_{eq}) for a perfect secondary path model, as a factor limiting the convergence behavior of the FxLMS algorithm. In fact, the expression given in (34) is an extension of previously-derived expressions to a more general case with $\hat{\mathbf{s}} \neq \mathbf{s}$. It can be seen that by setting $\hat{\mathbf{s}} = \mathbf{s}$, (34) is simplified to

$$\Delta_{eq} = \frac{\mathbf{s}^T\mathbf{\Psi}_Q\mathbf{s}}{\|\mathbf{s}\|^2} \tag{35}$$

which is similar to the expression derived in [14]. Note that when the model, obtained by the secondary path identification technique, is in form of $\hat{\mathbf{s}} = k\mathbf{s}$ (where k is a scalar), then the influence of the model misadjustment on the system performance can be effectively removed by scaling the adaptation step-size by a factor of $1/k$. This is because, in this case, the FxLMS update equation becomes

$$\mathbf{w}(n+1) = \mathbf{w}(n) + \mu k e(n)\mathbf{x}_f(n). \tag{36}$$

Therefore, it can be assumed that the system model, used in computation of $\mathbf{x}_f(n)$ is a perfect model and the adaptation step-size in increased by a factor of k. However, the misadjustment of the model, usually obtained by a secondary path identification technique, is more complicated in practice. In fact if the model is in form of $\hat{\mathbf{s}} = k\mathbf{s}$, it can be considered as a perfect model. This paper aims at considering a general case with an arbitrary imperfect secondary path model.

IV. Performance Analysis

The dynamic model for the excess-MSE function, given in (31), can be interpreted as the distance of the instantaneous power of the residual noise from the minimum achievable noise power. Based on this interpretation, performance of ANC systems in both the transient and steady-state modes can be studied by analyzing the variation of this function during the operation of the adaptation algorithm. This section used the model, developed for the excess-MSE function in Section III, to determine influences of imperfect secondary path models on stability, steady-state and convergence speed of FxLMS-based ANC systems. Note that, in ANC literature, the excess-MSE level is usually referred to as the distance of the residual noise power from its minimum level in steady state conditions [20], [21]. However, the variation of excess-MSE in both the transient and steady-state modes is studied in this paper. For this reason, the term "excess-MSE function" is used in this paper (rather than "excess-MSE").

A. Stability

Equation (24) shows that $J_{ex}(n)$ is a positive definite function of adaptation process variables. Therefore, according to the Lyapunov stability theory, if $\triangle J_{ex}(n) < 0$ then $J_{ex}(n)$ is a Lyapunov function and the adaptation process converges to its equilibrium point at origin: $\mathbf{c}(n) \rightarrow \mathbf{0}$, corresponding to $\mathbf{w}(n) \rightarrow \mathbf{w}_o$. In transient conditions, the MSE function is far from its optimal level: $J(n) \gg J_{\min}$. In this case, the first term in (27) can be neglected and, thereby, (31) can be approximated by

$$\triangle J_{ex}(n) \approx -\mu\sigma_x^2\|\hat{\mathbf{s}}\|^2\hat{\beta}\mathcal{J}(n). \tag{37}$$

According to (28), $\mathcal{J}(n)$ is positive definite (because $\forall n, J_{ex}(n) > 0$). In this case, $\triangle J_{ex}(n) < 0$ holds if

$$\hat{\beta} > 0. \tag{38}$$

From (33), it can be obtained that if μ is smaller than the following upper-bound (hereafter called the stability bound) then $\hat{\beta} > 0$ and, thereby, the convergence of the adaptation process to its equilibrium point is assured

$$\hat{\mu}_{\max} = \frac{2\mathbf{s}^T\hat{\mathbf{s}}}{\sigma_x^2\|\mathbf{s}\|^2\|\hat{\mathbf{s}}\|^2(L + 2\hat{\Delta}_{eq})}. \tag{39}$$

By setting $\hat{\mathbf{s}} = \mathbf{s}$ in (39), the stability bound of the system with a perfect secondary path model (denoted by $\mu_{\max}$) can be obtained as

$$\mu_{\max} = \frac{2}{\sigma_x^2\|\mathbf{s}\|^2(L + 2\Delta_{eq})}. \tag{40}$$

A similar expression for $\mu_{\max}$ was derived in [14]. Generally, the stability bound is a factor limiting the stability of an FxLMS-based ANC system. Therefore, in order to investigate the influence of an arbitrary secondary path model on stability of ANC systems, the ratio of $\hat{\mu}_{\max}$ to $\mu_{\max}$, called the stability ratio, can be evaluated. This ratio is defined as

$$r_\mu \triangleq \frac{\hat{\mu}_{\max}}{\mu_{\max}}. \tag{41}$$

By using (39) and (40), r_μ can be obtained as

$$r_\mu = \frac{\mathbf{s}^T\hat{\mathbf{s}}}{\|\hat{\mathbf{s}}\|^2}\left(\frac{L + 2\Delta_{eq}}{L + 2\hat{\Delta}_{eq}}\right). \tag{42}$$

In practice, high order adaptive filters are used (large L). In this case, (42) can be approximated by

$$r_\mu \approx \frac{\mathbf{s}^T\hat{\mathbf{s}}}{\|\hat{\mathbf{s}}\|^2}. \tag{43}$$

By using (41) and (43), influences of imperfect secondary path models on stability bound of FxLMS-based ANC systems can be investigated in the following three different cases.

Case A1) When the correlation of the actual secondary path and its model is negative: $\mathbf{s}^T\hat{\mathbf{s}} < 0$, the stability

ratio becomes negative: $r_\mu < 0$. From (40), it can be seen that $\mu_{\max}$ is always positive; therefore, combining the inequality of $r_\mu < 0$ and (41) results in

$$r_\mu < 0 \Rightarrow \hat{\mu}_{\max} < 0 \tag{44}$$

which means that there is no positive step-size for which the system becomes stable.

Case A2) When $0 < \mathbf{s}^T\hat{\mathbf{s}} < \|\hat{\mathbf{s}}\|^2$, the stability ratio has a value between 0 and 1: $0 < r_\mu < 1$. In this case, $\hat{\mu}_{\max}$ is smaller than $\mu_{\max}$; therefore, the system can still become stable (for $\mu < \hat{\mu}_{\max}$) but its stability bound is decreased by a factor of r_μ.

Case A3) When $\mathbf{s}^T\hat{\mathbf{s}} > \|\hat{\mathbf{s}}\|^2$, the stability ratio becomes greater than 1: $r_\mu > 1$. Accordingly, $\hat{\mu}_{\max}$ becomes than $\mu_{\max}$. In this case, the imperfect secondary path model causes the stability bound of the system to be increased (by a factor of r_μ). The maximum possible value of r_μ can be computed from the Cauchy Schawrs inequality as

$$\frac{\mathbf{s}^T\hat{\mathbf{s}}}{\|\mathbf{s}\|\|\hat{\mathbf{s}}\|} < 1 \Rightarrow \max r_\mu = \frac{\|\mathbf{s}\|}{\|\hat{\mathbf{s}}\|}. \tag{45}$$

Therefore, the necessary condition for occurring this case (increasing the stability bound by the imperfect secondary path model) is

$$\max r_\mu > 1 \Rightarrow \|\mathbf{s}\| > \|\hat{\mathbf{s}}\|. \tag{46}$$

B. Steady-State Performance

In steady-state conditions, the time difference of the excess-MSE becomes zero

$$\lim_{n\to\infty} \triangle J_{ex}(n) = 0 \tag{47}$$

where $J_{ex}(\infty)$ denotes the steady-state excess-MSE. Substituting (28) and (31) into (47) results in

$$\alpha J_{\min} = \hat{\beta} \sum_{q=0}^{Q-1} s_q^2 J_{ex}(\infty). \tag{48}$$

By solving (48), $J_{ex}(\infty)$ is obtained as

$$J_{ex}(\infty) = \frac{\alpha J_{\min}}{\hat{\beta}\|\mathbf{s}\|^2}. \tag{49}$$

By substituting (32) and (33) into (49) and simplifying the result, $J_{ex}(\infty)$ is obtained as

$$J_{ex}(\infty) = \frac{\mu L \sigma_x^2 J_{\min}}{2\frac{\mathbf{s}^T\hat{\mathbf{s}}}{\|\mathbf{s}\|^2\|\hat{\mathbf{s}}\|^2} - \mu\sigma_x^2(L + 2\hat{\Delta}_{eq})}. \tag{50}$$

Combining (39) and (50) results in

$$J_{ex}(\infty) = \frac{0.5\mu L \sigma_x^2 J_{\min}}{\frac{\mathbf{s}^T\hat{\mathbf{s}}}{\|\mathbf{s}\|^2\|\hat{\mathbf{s}}\|^2}\left(1 - \frac{\mu}{\hat{\mu}_{\max}}\right)}. \tag{51}$$

For relatively small step-sizes ($\mu \ll \hat{\mu}_{\max}$), $J_{ex}(\infty)$ can be approximated by

$$J_{ex}(\infty) = 0.5\mu L \sigma_x^2 \frac{\|\mathbf{s}\|^2\|\hat{\mathbf{s}}\|^2}{\mathbf{s}^T\hat{\mathbf{s}}} J_{\min}. \tag{52}$$

In steady-state conditions, (23) can be re-expressed as

$$\hat{\mathcal{MSE}} = J_{\min} + J_{ex}(\infty) \tag{53}$$

where $\hat{\mathcal{MSE}}$ denotes the steady-state MSE. By substituting $J_{ex}(\infty)$ into (53), the steady-state MSE can be obtained as a function of step-size μ and secondary path model $\hat{\mathbf{s}}$:

$$\hat{\mathcal{MSE}} = J_{\min} + 0.5\mu L \sigma_x^2 \frac{\|\mathbf{s}\|^2\|\hat{\mathbf{s}}\|^2}{\mathbf{s}^T\hat{\mathbf{s}}} J_{\min}. \tag{54}$$

The steady-state MSE of the system using a prefect secondary path model (denoted by $\mathcal{MSE}$) can be obtained by setting $\hat{\mathbf{s}} = \mathbf{s}$ in (54) as

$$\mathcal{MSE} = J_{\min} + 0.5\mu L \sigma_x^2 \|\mathbf{s}\|^2 J_{\min}. \tag{55}$$

A similar expression for $\mathcal{MSE}$ was derived in [21]. The steady-state performance of an ANC system is inversely related to the steady-state MSE. Therefore, in order to investigate influences of a secondary path model on the steady-state performance of the system, the ratio of $\mathcal{MSE}$ to $\hat{\mathcal{MSE}}$ can be evaluated. This ratio, called the steady state performance ratio, is defined as

$$r_\infty \triangleq \frac{\mathcal{MSE}}{\hat{\mathcal{MSE}}}. \tag{56}$$

By using (54)–(56), r_∞ is obtained as

$$r_\infty = \frac{1 + 0.5\alpha}{1 + 0.5\alpha\frac{\|\hat{\mathbf{s}}\|^2}{\mathbf{s}^T\hat{\mathbf{s}}}} \tag{57}$$

where $\alpha = \mu L \sigma_x^2 \|\mathbf{s}\|^2$, as defined earlier in (32). By using (43), r_∞ is simplified to

$$r_\infty = \frac{1 + 0.5\alpha}{1 + \frac{0.5\alpha}{r_\mu}} \tag{58}$$

which shows the existence of a direct relationship between r_μ and r_∞. By using (56)–(58), influences of imperfect secondary path models on steady state performance of FxLMS-based ANC systems can be investigated in the following three different cases.

Case B1) When $r_\mu < 0$, the steady-state ratio varies from $-\infty$ to $+\infty$; however, since r_μ is negative, the system is unstable (referring to Case A1).

Case B2) When $0 < r_\mu < 1$, the steady state ratio has a value between 0 and 1: $0 < r_\infty < 1$. Therefore, the steady-state performance of the system is decreased (by a factor of r_∞).

Case B3) When $r_\mu > 1$, the steady state ratio becomes greater than 1: $r_\infty > 1$. In this case, the steady state performance of the system is increased (by a factor of r_∞). However, even for $r_\mu \to \infty$, the steady-state ratio cannot reach beyond $1 + (0.5\alpha)$.

C. Convergence Speed

According to the Lyapunov stability theory, the convergence speed of a dynamic system, is directly related to the absolute value of its Lyapunov function time difference. As mentioned in Section IV-A, the excess-MSE function is a Lyapunov function of system variables. Therefore, from (37), it can be shown that the convergence speed of FxLMS-based ANC systems has a direct relationship to $\|\hat{\mathbf{s}}\|^2\hat{\beta}$

$$\hat{\omega} \propto \|\hat{\mathbf{s}}\|^2\hat{\beta} \tag{59}$$

where $\hat{\omega}$ denotes the convergence speed of the system with imperfect secondary path models. For the convergence speed of the system with a perfect secondary path model (denoted by $\hat{\omega}$), this relation becomes

$$\omega \propto \|\mathbf{s}\|^2. \tag{60}$$

In order to investigate influence of an imperfect secondary path model on the convergence speed of ANC systems, the ratio of $\hat{\omega}$ to ω can be evaluated. This ratio, called the convergence speed ratio, is defined as

$$r_\omega \triangleq \frac{\hat{\omega}}{\omega}. \tag{61}$$

By using (33), r_ω is obtained as

$$r_\omega = \frac{2\frac{\mathbf{s}^T\hat{\mathbf{s}}}{\|\mathbf{s}\|^2} - \mu\sigma_x^2\|\hat{\mathbf{s}}\|^2(L+2\hat{\Delta}_{eq})}{2-\mu\sigma_x^2\|\mathbf{s}\|^2(L+2\Delta_{eq})} \tag{62}$$

which can be simplified to

$$r_\omega = \frac{\mathbf{s}^T\hat{\mathbf{s}}}{\|\mathbf{s}\|^2}\left(\frac{1-\frac{\mu}{\mu_{\max}}}{1-\frac{\mu}{\mu_{max}}}\right). \tag{63}$$

For small step-sizes, (63) can be approximated by

$$r_\omega \approx \frac{\mathbf{s}^T\hat{\mathbf{s}}}{\|\mathbf{s}\|^2}. \tag{64}$$

In practice, small step-sizes are used due to non-stationary behaviors of physical acoustic noise. Accordingly, (64) can efficiently evaluate r_ω in practical situation; however, (63) can perfectly evaluate this parameter for either a small or large step-size. Based on (61) and (64), influences of imperfect secondary path models on convergence speed of FxLMS-based ANC systems can be investigated in the following three different cases.

Case C1) When the correlation of the actual secondary path and its model is negative: $\mathbf{s}^T\hat{\mathbf{s}} < 0$, the convergence speed ratio becomes negative: $r_\omega < 0$. This conditions ($\mathbf{s}^T\hat{\mathbf{s}} < 0$) also satisfies $r_\mu < 0$; therefore, this case is equivalent to Case A1 in which the system becomes unstable.

Case C2) When $0 < \mathbf{s}^T\hat{\mathbf{s}} < \|\mathbf{s}\|^2$, the convergence speed ratio has a value between 0 and 1: $0 < r_\omega < 1$. In this case, $\hat{\omega}$ is smaller than ω; therefore, the convergence speed is decreased (by a factor of r_ω).

Case C3) When $\mathbf{s}^T\hat{\mathbf{s}} > \|\mathbf{s}\|^2$, the stability ratio becomes greater than 1: $r_\omega > 1$. Accordingly, $\hat{\omega}$ becomes greater than ω. In this case, the convergence speed of the system is increased by a factor of r_ω. The maximum possible value of r_ω can be computed from the Cauchy Schawrs inequality as

$$\max r_\omega = \frac{\|\hat{\mathbf{s}}\|}{\|\mathbf{s}\|} \tag{65}$$

which equals to the inverse of $\max r_\mu$. Therefore, the necessary (not sufficient) condition for occurring this case (increasing the convergence speed by the imperfect secondary path model) is

$$\max r_\omega > 1 \Rightarrow \|\mathbf{s}\| < \|\hat{\mathbf{s}}\|. \tag{66}$$

Comparing this case and Case A3 shows that occurrence of these two cases for a given secondary path model is impossible. This is because the necessary condition for the occurrence of Case B3 is $\|\mathbf{s}\| > \|\hat{\mathbf{s}}\|$ but the necessary condition for the occurrence of Case C3 is $\|\mathbf{s}\| < \|\hat{\mathbf{s}}\|$. As a result, it is not possible that a given imperfect secondary path model causes both the stability bound and convergence speed of FxLMS-based ANC systems to be improved.

V. Intentional Misadjustment of Secondary Path Models

From the above discussion, the following rules, governing influences of imperfect secondary path models on FxLMS-based ANC systems, can be derived.

Rule1) Case A1 occurs only when $r_\mu < 0$ holds, resulting in the occurrence of Case B1. Also, $r_\mu < 0 \Rightarrow \mathbf{s}^T\hat{\mathbf{s}} < 0$, resulting in the occurrence of Case C1.

Rule2) Case A2 occurs only when $0 < r_\mu < 1$ holds, resulting in the occurrence of Case B2.

Rule3) Case A3 occurs only when $r_\mu > 1$ holds, resulting in the occurrence of Case B3.

Rule4) The occurrence of Case A3 is possible if $\|\mathbf{s}\| > \|\hat{\mathbf{s}}\|$ holds; on the other hand the occurrence of Case C3 is possible if $\|\mathbf{s}\| < \|\hat{\mathbf{s}}\|$ holds. Therefore, Cases A3 and C3 can not occur with each other.

By applying these rules, influences of secondary path models on FxLMS-based ANC systems can be classified into four composite cases, as shown in Fig. 3. For each composite case, the behavior of the system is described in Table I. According to this table, the first composite case occurs when A1, B1, and C1 occur, resulting in the instability of the system due to the use of imperfect secondary path models. The second composite case corresponds to the occurrence of A2, B2, and C2, resulting in decrease in the stability-bound, steady state performance and convergence speed of the system. The third composite case occurs when A2, B2, and C3 occurs, resulting in decrease in the stability bound and steady state performance and increase in the convergence speed. Finally, the fourth composite case occurs when A3, B3, and C2 occur, resulting in increase in both the stability bound and steady-state performance and decrease in the convergence speed. However, as mentioned earlier, the steady-state performance can not considerably improve in this case.

As a surprising result, imperfect secondary path models do not necessarily degrade all of the stability bound, steady state performance or convergence speed of FxLMS-based ANC systems. Therefore, intentional misadjustment of secondary path

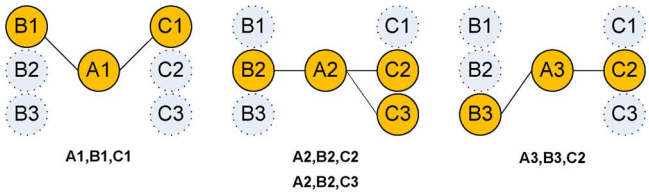

Fig. 3. Composite cases (possible combinations of cases).

TABLE I
COMPOSITE CASES OF INFLUENCES OF IMPERFECT SECONDARY PATH MODELS ON FXLMS-BASED ANC SYSTEMS

	Composite Case	Stability Condition	Steady State Performance	Convergence Speed
I	A1,B1,C1	unstable	-	-
II	A2,B2,C2	degraded	degraded	degraded
III	A2,B2,C3	degraded	slightly degraded	improved
IV	A3,B3,C2	improved	slightly improved	degraded

models can improve stability bound or steady state performance of these systems, at the cost of decreasing their convergence speed (the forth composite case). Also, it can improve convergence speed of these systems at the cost of degrading their stability bound and steady-state performance (the third composite case).

In practice, since small step-sizes are used ($\mu \ll \mu_{\max}$), the ANC system can easily tolerate a moderate decrease in the stability bound. For example, if the ratio of stability for a particular secondary path model is $r_\mu = 0.5$, then the stability bound is decreased by a factor of 0.5. However, since the step-size is adjusted far from the original $\mu_{\max}$, the new maximum bound does not result in instability. Moreover, it can be found out that, for small step-sizes, the ratio of steady-state performance always remains around 1. As a particular example, when $r_\mu = 0.5$, the steady-state ratio can be obtained from (58) as $r_\infty = (1 + 0.5\alpha)/(1 + \alpha)$, which is a number close to 1 (because small μ results in small α). Therefore, since the steady state performance is decreased by a factor of $r_\infty \approx 1$, its variation can be neglected. According to this discussion, it can be stated the the disadvantages of the third composite case can be tolerated by the practical ANC systems. Now, the question to be answered is: for a particular secondary path model with a stability ratio smaller than 1 (e.g., $r_\mu = 0.5$), how much improvement in the convergence speed is achievable? In other words, if the cost of using an imperfect secondary path model with a stability ratio smaller than 1 is justified, what is the maximum achievable benefit to the convergence speed?

From Cauchy–Schwarz inequality, it can be shown that

$$(\mathbf{s}^T\hat{\mathbf{s}})^2 < \|\hat{\mathbf{s}}\|^2\|\mathbf{s}\|^2 \Rightarrow \frac{\mathbf{s}^T\hat{\mathbf{s}}}{\|\mathbf{s}\|^2} < \frac{\|\hat{\mathbf{s}}\|^2}{\mathbf{s}^T\hat{\mathbf{s}}} \tag{67}$$

which is equivalent to

$$r_\omega < \frac{1}{r_\mu}. \tag{68}$$

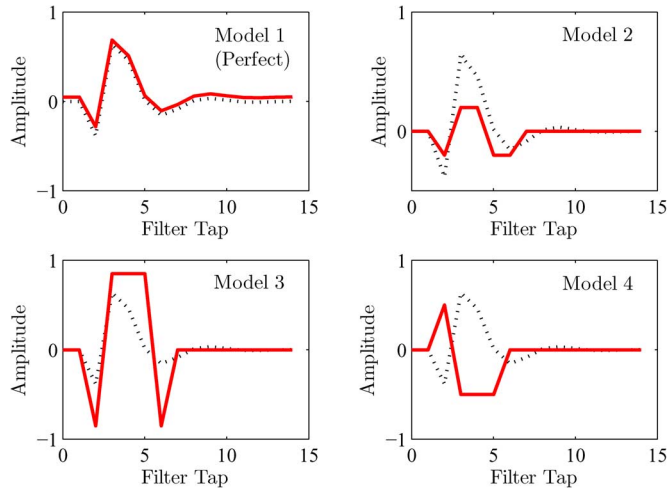

Fig. 4. Impulse responses of actual secondary path and its models used in computer simulation; dashed lines: actual system; solid lines: models.

Therefore, when the stability ratio is smaller than 1, the maximum achievable convergence speed ratio equals to the inverse of the stability ratio. In the above example, where $r_\mu = 0.5$, the maximum achievable convergence speed ratio is $r_\omega = 2$ and its thus expected that a suitable imperfect secondary path model can cause the convergence speed of the system to be increased by a factor of up to 2.

VI. SIMULATION RESULTS

Simulation results shows the validity of the proposed theoretical results. Fig. 4 shows the impulse response of the actual secondary path used in computer simulation, as well as those of 4 imperfect models of it. As can be seen, model 1 is a nearly perfect model but models 2, 3, and 4 are deviated from the perfect model. In simulation, the filter length is set to $L = 32$ and the primary noise $d(n)$ is a computer-generated white sequence of real numbers with mean zero and variance $\sigma_x^2 = 1$. In these conditions, the minimal MSE can be computed using (6) as $J_{\min} = 5 \times 10^{-3}$. For each model, ratios r_μ, r_∞, and r_ω can be computed by using (43), (58), and (64).

For model 1 (perfect model), all of the performance ratios are equal to one. Also, the equivalent delay of the secondary path can be obtained using (34) as $\Delta_{eq} = 3.22$, the upper-bound of the step-size can be obtained using (40) as $\mu_{\max} = 0.0652$, and the steady state MSE can be obtained using (55) as $\mathcal{MSE} = -22.95$ dB. These values can be considered as the reference values.

For model 2, the stability ratio is $r_\mu = 1.6216$, the steady-state ratio is $r_\infty = 1.0156$ and the convergence speed ratio is $r_\omega = 0.4066$. This situation is an example for the occurrence of the fourth composite case; it is thus expected that the stability bound is increased by a factor of 1.6216, the steady-state performance is slightly increased by a factor of 1.0156 and the convergence speed is decreased by a factor of 0.4066.

For model 3, the stability ratio is $r_\mu = 0.3880$, the steady-state ratio is $r_\infty = 0.9407$ and the convergence speed ratio is $r_\omega = 1.7575$. In this situation, the third composite case occurs. Consequently, it is expected that the stability bound is decreased by a factor of 0.3880, the steady-state performance is slightly

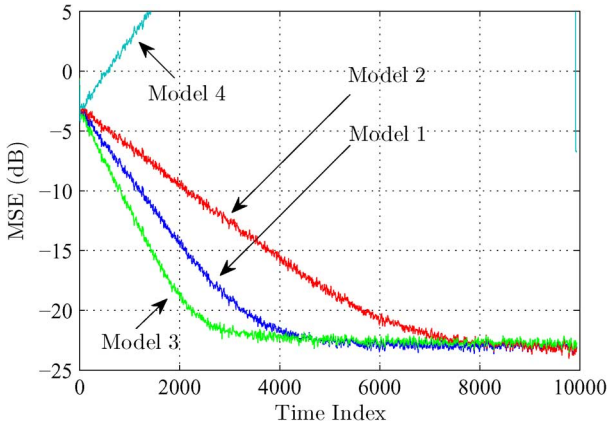

Fig. 5. Mean square error obtained from simulation experiments.

decreased by a factor of 0.9407 and the convergence speed is increased by a factor of 1.7575.

For model 4, the stability ratio is $r_\mu = -0.7472$, therefore, since the first composite case occurs, the system becomes unstable. For each model, the operation of the FxLMS-based ANC system is simulated in MATLAB. The MSE function is computed by averaging the square error signal over 200 different runs with independent sequences of noise. The result is plotted in Fig. 5. As can be seen, for all models, the result is in an excellent agreement with the analytical result. According to this figure, it is evident that the effect of using imperfect secondary path models on the convergence speed of FxLMS-based ANC systems is significant but this effect on steady-state performance of these systems is neglectable. The interesting result is gaining a convergence speed higher than the reference speed when imperfect model 3 is used.

VII. Experimental Results

Fig. 6 shows the schematic diagram of the experimental adaptive ANC setup in this research. Fig. 7 shows a photo of the actual system. The acoustic duct with dimensions of 150 cm $\times$31 cm $\times$ 23 cm is constructed from 1.8 cm thick medium density fiber-board, with carpeted interiors. This duct was equipped with the following electro-acoustic components:

1) reconfigurable field-programmable gate array (FPGA) Chassis (NI 9104), which utilizes an embedded Xilinx FPGA chip (clocked at 40 MHz);
2) 400 MHz high performance real-time digital controller (NI CRIO-9014) [22];
3) 24-Bit analog input module (NI 9233);
4) 16-Bit analog output modules (NI 9263);
5) two microphones with cardioid response pattern (AKG-D770), used as the reference and error microphones;
6) loudspeaker with on-board 20 W power amplifier (Phonic SEp 207), used as the anti-noise source.

The combination of the reconfigurable chassis, real-time controller, and I/O modules creates a complete stand-alone embedded system. The FPGA circuitry in the chassis controls each I/O module and passes data to the controllers through a local PCI bus using built-in communication functions. The FPGA design of the ANC system should be developed in *LAB VIEW FPGA Module* and compiled into a bit-stream file for download onto CRIO, where the design is synthesized in the FPGA

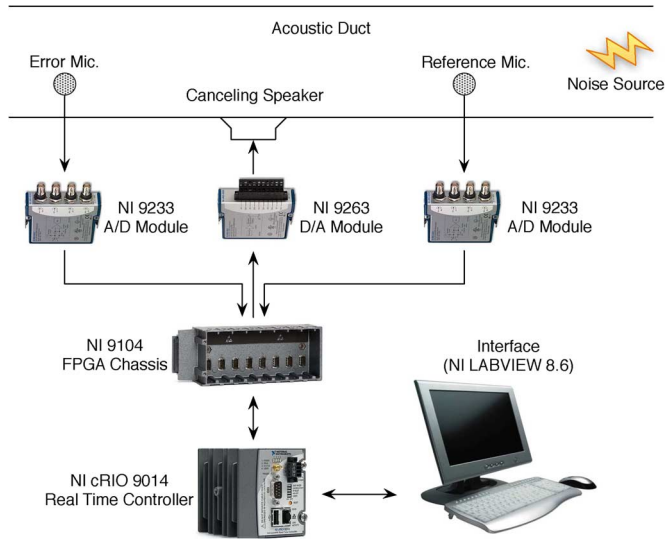

Fig. 6. Schematic diagram of experimental setup.

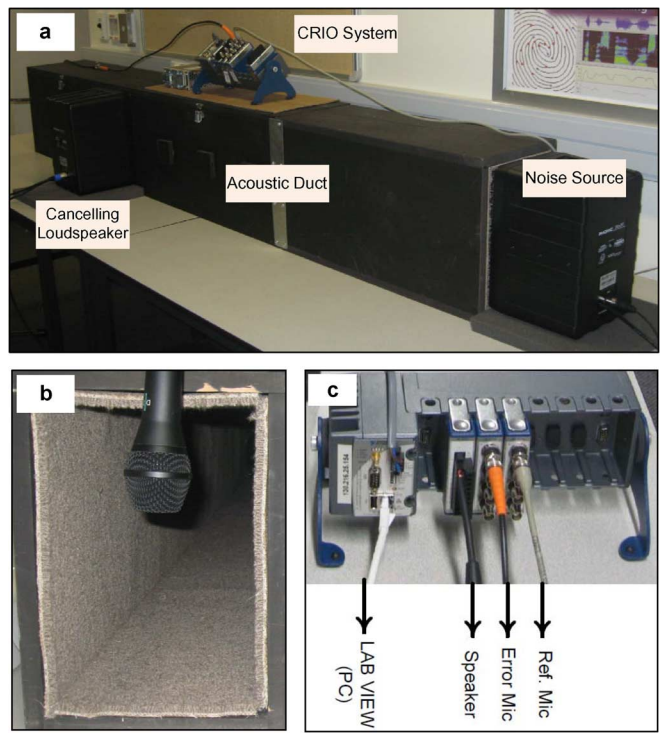

Fig. 7. Experimental setup: (a) general view, (b) interior view of acoustic duct, and (c) CRIO embedded system and its connections.

chip. The real-time system has two modules; the first of which is a real-time adaptive LMS algorithm for offline secondary path modeling. This model (which is assumed to be a perfect model) is then uploaded onto the memory of the FPGA chassis. The second module or main module, is a real-time adaptive FxLMS-based ANC system. Note that, in all the experiments, the step-size is set to a small number below than 0.1 $\mu_{\max}$; accordingly, (43), (58), and (64), which are derived assuming a small step size, are valid.

In the first experiment, the secondary path model (model 1 shown in Fig. 8 is the one uploaded in the memory before conducting the experiment. It can be assumed that this model is a perfect model; therefore all of the ratios are equal to one. The power of the residual noise obtained from this experiment is

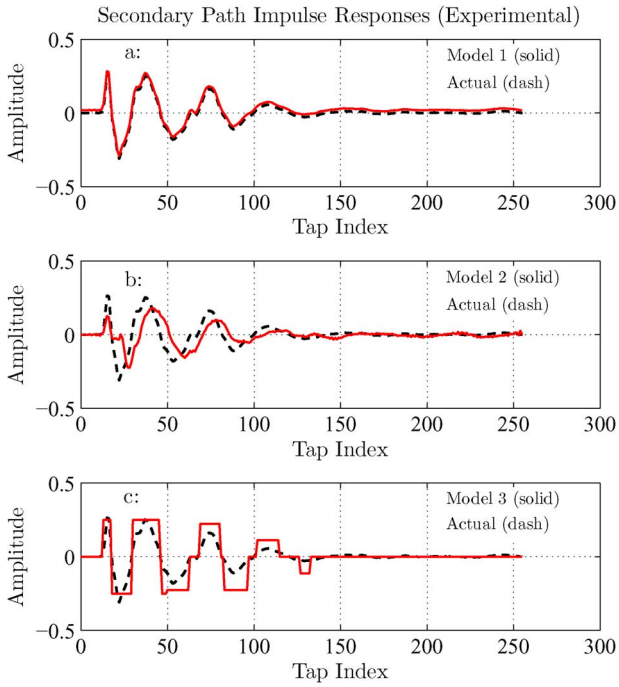

Fig. 8. Impulse responses of actual secondary path and its models in experiments; dashed lines: actual system; solid lines: estimated models.

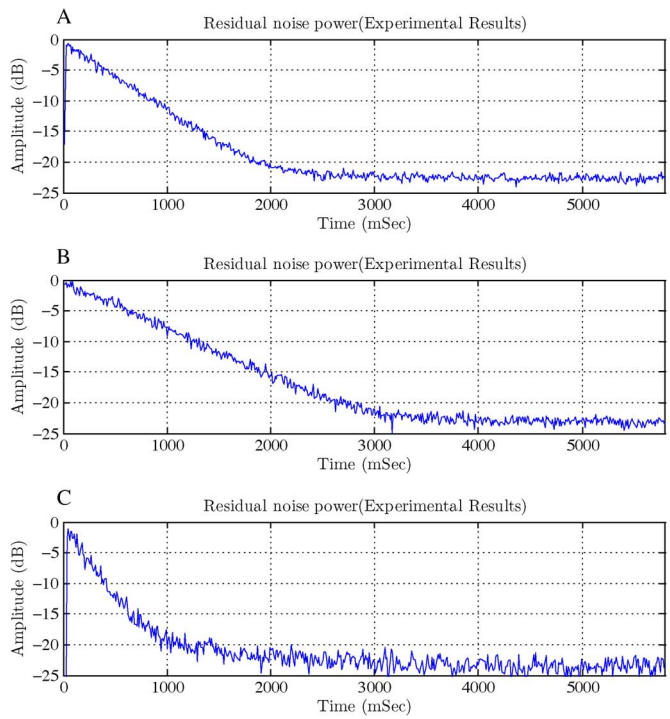

Fig. 9. Residual noise power obtained by using experimental ANC system.

shown in Fig. 9(a). As can be seen, the residual noise power converges to -22 dB after about 1900 ms. This result is considered as the reference result for the next experiments.

In the second experiment, the position of the error microphone is unchanged; therefore, the actual secondary path remains identical to that of the previous experiment. However, an imperfect secondary path model with the impulse response, shown in Fig. 8 (model 2) is used. By using (43), (58), and (64) the ratios of imperfect secondary path model can be obtained as $r_\mu = 0.7600$, $r_\infty = 0.9934$ and $r_\omega = 0.5816$. Therefore; it is expected that, the convergence speed of the system is decreased and its steady state performance remains untouched. The power of the residual noise obtained from this experiment is shown in Fig. 9(b). As can be seen, this signal power reach about the reference level of -22 dB after about 3000 ms.

In the third experiment, the secondary path model is intentionally adjusted to model 3 (shown in Fig. 8. However, since the error microphone position is unchanged the actual secondary path remains constant. For the secondary path model used in this experiment, $r_\mu = 0.5461$, $r_\infty = 0.9821$, and $r_\omega = 1.5479$. Therefore, it is expected that the steady state performance of the system remains untouched but its convergence speed is increased by a factor of about 1.5479. The power of the residual noise obtained from this experiment is shown in Fig. 9(c). According to this figure, the residual noise power reach about the reference level of -22 dB after about 1200 ms. As expected, intentional misadjustment of the secondary path model into model 3, causes the overall performance of the ANC system to be improved.

VIII. Conclusion

The stochastic analysis of the FxLMS-based ANC systems, conducted in the authors previous work, has a good potential to be extended for more general cases. As an effort to extend this analysis, it is assumed that the secondary path model used by the FxLMS algorithm is not a perfect model. The results obtained from this analysis consists of a number of mathematical expression, describing influences of imperfect secondary path models on the stability bound, steady-state performance and convergence speed of FxLMS-based ANC system. As a surprising result, it is found out that intentional misadjustment of secondary path models can improve convergence rate of these systems at the cost of decreasing their stability bound and steady-state performance. It is shown that the moderate decrease of the stability bound is tolerable and, also, the effects of imperfect secondary path model on the steady-state performance is not considerable. Therefore, it is suggested to improve the convergence speed of the FxLMS-based ANC systems by misadjusting the secondary path model used in the FxLMS algorithm.

Appendix A
Computation of $\hat{A}(n)$

By defining

$$\hat{a}(n) \triangleq \sigma_x^2 E\left\{\hat{\mathbf{z}}_f^T(n)\hat{\mathbf{z}}_f(n)e^2(n)\right\}. \tag{69}$$

$\hat{A}(n)$ can be expressed as

$$\hat{A}(n) = \mu^2 \sum_{q=0}^{Q-1} s_q^2 \hat{a}(n-q). \tag{70}$$

Assuming that the data sequence (reference signal) is independent of the MSE function, and using (23), $\hat{a}(n)$ is simplified to

$$\hat{a}(n) = \sigma_x^2 \underbrace{E\left\{\hat{\mathbf{z}}_f^T(n)\hat{\mathbf{z}}_f(n)\right\}}_{v(n)} \left(\hat{J}_{\min} + J_{ex}(n)\right). \tag{71}$$

From (14) and (20), the term $\upsilon(n) = E\{\hat{\mathbf{z}}_f^T(n)\hat{\mathbf{z}}_f(n)\}$ appeared in (71) can be expanded to

$$\upsilon(n) = \sum_{m,k=0}^{Q-1}\sum_{l=0}^{L-1} \hat{s}_m\hat{s}_k E\left\{z_l(n-m)z_l(n-k)\right\}. \quad (72)$$

Substituting (15) into (72) results in

$$\upsilon(n) = \sum_{m,k=0}^{Q-1}\sum_{l=0}^{L-1} \hat{s}_m\hat{s}_k \mathbf{F}_l^T E\left\{\mathbf{x}(n-m)\mathbf{x}^T(n-k)\right\}\mathbf{F}_l. \quad (73)$$

Now, combining (21) and (73) results in

$$\upsilon(n) = \sum_{m=0}^{Q-1}\sum_{l=0}^{L-1} \hat{s}_m^2 \mathbf{F}_l^T\mathbf{R}\mathbf{F}_l. \quad (74)$$

From (11) $\mathbf{F}_l^T\mathbf{R}\mathbf{F}_l = \sigma_x^2$; therefore

$$\upsilon(n) = L\sigma_x^2\sum_{m=0}^{Q-1}\hat{s}_m^2 = L\sigma_x^2\|\hat{\mathbf{s}}\|^2 \quad (75)$$

where $\|.\|$ denotes the vector norm and vector $\hat{\mathbf{s}}$ is defined in (2). Now, combining (71) and (75) results in

$$\hat{a}(n) = L\sigma_x^4\|\hat{\mathbf{s}}\|^2\hat{J}_{\min} + L\sigma_x^4\|\hat{\mathbf{s}}\|^2 J_{ex}(n). \quad (76)$$

Subsequently, combining (76) and (70) gives $\hat{A}(n)$ as shown in (27).

Appendix B
Computation of $\hat{B}(n)$

By defining

$$\hat{b}(n) \stackrel{\text{def}}{=} \sigma_x^2 E\left\{\mathbf{c}^T(n)\hat{\mathbf{z}}_f(n)e(n)\right\}. \quad (77)$$

$\hat{B}(n)$ can be expressed as

$$\hat{B}(n) = 2\mu\sum_{q=0}^{Q-1} s_q^2\hat{b}(n-q). \quad (78)$$

Using (18), $\hat{b}(n)$ can be expanded to

$$\begin{aligned}\hat{b}(n) = {} & \sigma_x^2 E\left\{\mathbf{c}^T(n)\hat{\mathbf{z}}_f(n)\hat{e}_o(n)\right\} \\ & - \sigma_x^2\sum_{p=0}^{Q-1} s_p E\left\{\mathbf{c}^T(n)\hat{\mathbf{z}}_f(n)\mathbf{z}^T(n-p)\mathbf{c}(n-p)\right\}. \quad (79)\end{aligned}$$

The first term is zero because according to the second and third independence assumptions the reference signal is a zero mean signal and independent of the weight vector and the optimum error. Therefore, $\hat{b}(n)$ can be simplified as

$$\begin{aligned}\hat{b}(n) = {} & -\sigma_x^2\sum_{p=0}^{Q-1}\sum_{m=0}^{M-1} s_p\hat{s}_m E\left\{\mathbf{c}^T(n)\mathbf{z}(n-m)\mathbf{z}^T\right. \\ & \left.\times(n-p)\mathbf{c}(n-p)\right\} \\ = {} & -\sigma_x^2\sum_{p=0}^{Q-1}\sum_{m=0}^{M-1}\sum_{i,j=0}^{L-1} s_p\hat{s}_m E\left\{c_i(n)c_j(n-p)\right\} \\ & \times \mathbf{F}_i^T E\left\{\mathbf{x}(n-m)\mathbf{x}^T(n-p)\right\}\mathbf{F}_j \\ = {} & -\sigma_x^2\sum_{m=0}^{M-1}\sum_{i,j=0}^{L-1} s_m\hat{s}_m E\left\{c_i(n)c_j(n-p)\right\}\mathbf{F}_i^T\mathbf{R}\mathbf{F}_j.\end{aligned}$$

From (11) it can be obtained that $\mathbf{F}_i^T\mathbf{R}\mathbf{F}_j = \sigma_x^2\delta_{i,j}$. Using this identity in the above expression for $\hat{b}(n)$ results in

$$\hat{b}(n) = -\sigma_x^4\sum_{m=0}^{Q-1}\sum_{i=0}^{L-1} s_m\hat{s}_m E\left\{c_i(n)c_i(n-m)\right\} \quad (80)$$

which can be expressed as

$$\hat{b}(n) = -\sigma_x^2\sum_{m=0}^{Q-1} s_m\hat{s}_m r_m(n) \quad (81)$$

where $r_m(n)$ is defined as

$$r_m(n) \stackrel{\Delta}{=} \sigma_x^2 E\left\{\mathbf{c}^T(n)\mathbf{c}(n-m)\right\}. \quad (82)$$

In [14], it was shown that

$$r_m(n) = \sigma_x^2 E\left\{\mathbf{c}^T(n-m)\mathbf{c}(n-m)\right\} + m\mu b(n-m). \quad (83)$$

Now, combining (81) and (83) results in

$$\hat{b}(n) = -\sigma_x^2\hat{J}_{ex}(n) - \mu\sigma_x^2\sum_{m=0}^{Q-1} m s_m\hat{s}_m b(n-m) \quad (84)$$

where $\hat{J}_{ex}(n)$ is defined as

$$\hat{J}_{ex}(n) \stackrel{\Delta}{=} \sigma_x^2\sum_{m=0}^{Q-1} s_m\hat{s}_m E\left\{\mathbf{c}^T(n-m)\mathbf{c}(n-m)\right\}. \quad (85)$$

For slow adaptation process, it can be assumed that $E\{\mathbf{c}^T(n-m)\mathbf{c}(n-m)\} \approx E\{\mathbf{c}^T(n)\mathbf{c}(n)\}$; therefore, from (24) and (85) it can be approximately obtained that

$$\hat{J}_{ex}(n) \approx \frac{\sum_{m=0}^{Q-1} s_m\hat{s}_m}{\|\mathbf{s}\|^2} J_{ex}(n) = \frac{\mathbf{s}^T\hat{\mathbf{s}}}{\|\mathbf{s}\|^2} J_{ex}(n). \quad (86)$$

Using the approximation given in (86), (84) is simplified to

$$\hat{b}(n) = -\sigma_x^2\frac{\mathbf{s}^T\hat{\mathbf{s}}}{\|\mathbf{s}\|^2} J_{ex}(n) - \mu\sigma_x^2\sum_{m=0}^{Q-1} m s_m\hat{s}_m b(n-m). \quad (87)$$

Using the recursive property of (87), $\hat{b}(n)$ is expanded to

$$\begin{aligned}\hat{b}(n) = & -\sigma_x^2 \frac{\mathbf{s}^T\hat{\mathbf{s}}}{\|\mathbf{s}\|^2} J_{ex}(n) \\ & + \mu\sigma_x^4 \frac{\mathbf{s}^T\hat{\mathbf{s}}}{\|\mathbf{s}\|^2} \sum_{m=0}^{Q-1} m s_m \hat{s}_m J_{ex}(n-m) \\ & - \mu^2\sigma_x^6 \frac{\mathbf{s}^T\hat{\mathbf{s}}}{\|\mathbf{s}\|^2} \sum_{m,k=0}^{Q-1} mk s_m \hat{s}_m s_k \hat{s}_k J_{ex}(n-m-k). \\ & \vdots \end{aligned} \tag{88}$$

Since $\mu \ll 1$, $\hat{b}(n)$ can be approximated by its two first terms

$$\hat{b}(n) \approx -\sigma_x^2 \frac{\mathbf{s}^T\hat{\mathbf{s}}}{\|\mathbf{s}\|^2} \left(J_{ex}(n) - \mu\sigma_x^2 \sum_{m=0}^{Q-1} m s_m \hat{s}_m J_{ex}(n-m) \right). \tag{89}$$

Now, substituting $\hat{b}(n)$ into (78), $\hat{B}(n)$ is obtained as

$$\begin{aligned}\hat{B}(n) = -2\mu\sigma_x^2 \frac{\mathbf{s}^T\hat{\mathbf{s}}}{\|\mathbf{s}\|^2} \Bigg(& \sum_{q=0}^{Q-1} s_q^2 J_{ex}(n-q) \\ & -\mu\sigma_x^2 \sum_{q,m=0}^{Q-1} m s_m \hat{s}_m s_q^2 J_{ex}(n-q-m) \Bigg). \end{aligned} \tag{90}$$

For slow adaptation process, it can be approximately assumed that $J_{ex}(n-q-m) \approx J_{ex}(n-q)$, so (90) can be approximated by

$$\hat{B}(n) = -2\mu\sigma_x^2 \frac{\mathbf{s}^T\hat{\mathbf{s}}}{\|\mathbf{s}\|^2} \left(1 - \mu\sigma_x^2 \mathbf{s}^T \mathbf{\Psi}_Q \hat{\mathbf{s}}\right) \sum_{q=0}^{Q-1} s_q^2 J_{ex}(n-q) \tag{91}$$

where constant matrix $\mathbf{\Psi}_Q$ is defined in (30). Using this matrix, it can be shown that

$$\mathbf{s}^T \mathbf{\Psi}_Q \hat{\mathbf{s}} = \sum_{q=0}^{Q-1} q s_q \hat{s}_q. \tag{92}$$

Finally, $\hat{B}(n)$ can be expressed as shown in (29).

REFERENCES

[1] H. F. Olsen and E. G. May, "Electronic sound absorber," *J. Acoustical Soc. Amer.*, vol. 25, pp. 1130–1136, Nov. 1953.

[2] B. Widrow, J. Glover, J. McCool, J. Kaunitz, C. Williams, R. Hearn, J. Zeidler, J. Eugene Dong, and R. Goodlin, "Adaptive noise cancelling: Principles and applications," *Proc. IEEE*, vol. 63, no. 12, pp. 1692–1716, Dec. 1975.

[3] D. R. Morgan, "An analysis of multiple correlation cancellation loops with a filter in the auxiliary path," in *Proc. IEEE Int. Conf. Acoust., Speech, Signal Process. (ICASSP)*, 1980, pp. 457–461.

[4] J. C. Burgess, "Active adaptive sound control in a duct: Computer simulation," *J. Acoust. Soc. Amer.*, vol. 70, pp. 715–726, 1981.

[5] B. Widrow, D. Shur, and S. Shaffer, "On adaptive inverse control," in *Proc. 15th Asilomar Conf. Circuits, Syst., Comput.*, 1981, pp. 185–189.

[6] L. J. Eriksson and M. C. Allie, "Use of random noise for on-line transducer modeling in an adaptive active attenuation system," *J. Acoust. Soc. Amer.*, vol. 85, no. 2, pp. 797–802, Feb. 1989.

[7] M. Zhang, H. Lan, and W. Ser, "Cross-updated active noise control system with online secondary path modeling," *IEEE Trans. Speech Audio Process.*, vol. 9, no. 5, pp. 598–602, Jul. 2001.

[8] M. T. Akhtar, M. Abe, and M. Kawamata, "A new structure for feedforward active noise control systems with improved online secondary path modeling," *IEEE Trans. Speech Audio Process.*, vol. 13, no. 5, pp. 1082–1088, Sep. 2005.

[9] G. Long, F. Ling, and J. Proakis, "The LMS algorithm with delayed coefficient adaptation," *IEEE Trans. Acoust., Speech, Signal Process.*, vol. 37, no. 9, pp. 1397–1405, Sep. 1989.

[10] G. Long, F. Ling, and J. Proakis, "Corrections to 'The LMS algorithm with delayed coefficient adaptation'," *IEEE Trans. Signal Process.*, vol. 40, no. 1, pp. 230–232, Jan. 1992.

[11] E. Bjarnason, "Analysis of the filtered-x LMS algorithm," *IEEE Trans. Speech Audio Process.*, vol. 3, no. 6, pp. 504–514, Nov. 1995.

[12] L. Vicente and Masgrau, "Novel FxLMS convergence condition with deterministic reference," *IEEE Trans. Signal Process.*, vol. 54, no. 10, pp. 3768–3774, Oct. 2006.

[13] Y. Xiao, A. Ikuta, L. Ma, and K. Khorasani, "Stochastic analysis of the FXLMS-based narrowband active noise control system," *IEEE Trans. Audio, Speech, Lang. Process.*, vol. 16, no. 5, pp. 1000–1014, Jul. 2008.

[14] I. Tabatabaei Ardekani and W. Abdulla, "Theoretical convergence analysis of FxLMS algorithm," *Signal Process.*, vol. 90, no. 12, pp. 3046–3055, Dec. 2010.

[15] I. Tabatabaei Ardekani and W. Abdulla, "On the stability of adaptation process in active noise control systems," *J. Acoust. Soc. Amer.*, vol. 129, no. 1, pp. 173–185, Jan. 2011.

[16] S. Snyder and C. Hansen, "The effect of transfer function estimation errors on the filtered-x LMS algorithm," *IEEE Trans. Signal Process.*, vol. 42, no. 4, pp. 950–953, Apr. 1994.

[17] L. Wang and W.-S. Gan, "Convergence analysis of narrowband active noise equalizer system under imperfect secondary path estimation," *IEEE Trans. Audio, Speech, Lang. Process.*, vol. 17, no. 4, pp. 566–571, May 2009.

[18] S. Haykin, *Adaptive Filter Theory*, 4th ed. Englewood Cliffs, NJ: Prentice Hall, 2002.

[19] W. A. Gardner, "Learning characteristics of stochastic gradient descent algorithm: A general study, analysis and critique," *Int. J. Signal Process.*, vol. 6, pp. 113–133, 1984.

[20] S. M. Kuo and D. R. Morgan, *Active Noise Control Systems: Algorithms and DSP Implementations*. New York: Wiley Interscience, 1996.

[21] A. H. Sayed, *Adaptive Filters*. New York: Wiley Interscience, 2008.

[22] National Instruments Corp., Austin, TX, "CompactRIO-9012/9014 operating instructions and specifications," May 2008.

Iman Tabatabaei Ardekani (S'11) received the B.Sc. and M.Sc. degrees from the University of Tehran, Iran, in 2000 and 2003, respectively. Currently, he is pursuing the Ph.D. degree from the Electrical and Computer Engineering Department, The University of Auckland, New Zealand.

His research interests include adaptive control, statistical signal processing, and acoustics. He has published over 26 papers in different journals and international conferences.

Waleed H. Abdulla (M'06) received the Ph.D. degree from the University of Otago, Otago, New Zealand.

He has been working since 2002 as a Senior Lecturer with the Department of Electrical and Computer Engineering, the University of Auckland, Auckland, New Zealand. He is a visiting researcher/collaborator to many universities. He has published over 85 refereed publications including a patent and a book. He has supervised more than 25 postgraduate students.

Dr. Abdulla is a member of the editorial boards of IET Signal Processing Journal, The Open Signal Processing Journal, International Journal of Biometrics and International Journal of Bio-Science and Bio-Technology. He is a founder member of Asia-Pacific Association for Signal and Information Processing (APSIPA). He has leading roles in many conferences and international activities. He was a recipient of many awards and funded projects exceeding $900K. Recently, he has been awarded JSPS, ETRI, and HKPU fellowships and also an Excellent Teaching Award for 2005. He is a member of APSIPA.